The curious relationship of sintering to activity in supported gold catalysts for the hydrochlorination of acetylene

Kerry C. O'Connell, John R. Monnier, J.R. Regalbuto[*]

Department of Chemical Engineering, University of South Carolina, 301 Main St Columbia, SC 29208, United States

ABSTRACT

Gold catalysts for the hydrochlorination of acetylene are currently being studied as an environmentally benign replacement for industrial mercuric chloride catalysts, which undergo reduction and subsequent sublimation into the atmosphere. In this work the method of strong electrostatic adsorption was used with a cationic gold precursor to controllably deposit the gold precursors over a variety of activated carbon and metal oxide supports. The catalysts were characterized by XRD, STEM, and XPS before and after reaction or aging at temperature (180 °C) in HCl.

The synthesis procedure resulted in highly dispersed Au nanoparticles (usually below the 1.5 nm limit of detection and some from 2 to 3 nm) over all supports. The series of catalysts exhibited an unusual relationship of sintering to activity; the catalysts which best anchored the Au crystallites were the least active; titania and silica catalysts showed almost no sintering and were virtually inactive, and even a graphitic carbon catalyst exhibited good anchoring but very poor activity. The sintering was caused by the HCl atmosphere and not the temperature; catalysts submitted to the reaction temperature in He were stable.

It would appear that the metal nanoparticles, and Au at the edges of metal nanoparticles, are inactive. The current results support recent reports in the literature that the active sites are derived from isolated Au ions, but we can conclude that oxidized amorphous carbon also plays a key role in generating the active site. In this environment the active species is highly mobile and susceptible to sintering.

1. Introduction

Acetylene hydrochlorination is a catalytic synthesis route for the production of vinyl chloride monomer (VCM) which is common in coal-rich regions of the world, due to the facile production of acetylene from coal. The direct hydrochlorination of acetylene results in minimal need for separation after reaction, due to high selectivity to VCM [1]. The most common commercial catalyst for this reaction is carbon-supported mercuric chloride, which has significant environmental concerns − mainly the sublimation of reduced Hg^0 into the atmosphere due to hotspot formation during reaction. This loss of active metal, due to elevated vapor pressure, has raised environmental concerns as well as reduced the catalytic lifetime [2–4]. Research for a suitable replacement of mercury-containing catalysts for acetylene hydrochlorination continues to grow.

Many studies have focused on Au as an environmentally benign replacement [3,5–16]. There has been considerable interest in other single metal catalysts such as Pd^{2+} [17,18], Pt^{2+} [19,20], Cu^{2+} [21], Ru^{3+} [22–24], and Bi^{3+} [25] and more recently, novel nonmetallic

materials such as carbon nitride and boron-doped carbon and graphene [22,26,27]. Significant work has been done on modifying carbon support surfaces with oxygen-containing functional groups via chemical treatments with an oxidant, as well as thermal treatments, to adjust the ratio of those groups on the surface to investigate their role in the reaction mechanism [5,28,29]. Particle growth has a strong dependence on the concentration of HCl [30]. There is some precedent in the literature that the addition of surface functional groups through oxidation or nitrogen modification hinders catalyst deactivation [20,31–33].

Bimetallic systems have been explored to improve stability, such as gold and ruthenium or copper supported on carbon [2,11,18,24] or the addition of bismuth as a promoter to lessen the reduction of Au^{3+} to Au^{+1} instead of to Au^0 [34]. Reviewed in [11], bimetallics have to date failed to improve performance versus gold.

The active Au site for this reaction has not been precisely determined. While some works have ascribed activity to Au metal nanoparticles [35], others have suggested that a subset of metallic nanoparticles do not take place in the reaction [32]. Other evidence suggests that the active site involves the Au/C interface [5,32]. Two of the most

recent papers on Au-based catalysts contain descriptions of commercial demonstrations [11,12] in which low loading Au is particularly active, and the latest characterization is homing in on Au^{3+}/Au^{1+} couples as the active sites [11,14,15]. These can be stabilized and promoted by soft ligands such as thiosulfate and thiocyanate [11,12]. Furthermore, operando EXAFS and XANES have been used to demonstrate the active sites are isolated Au ions [15], which inherently involves the Au/carbon interface. However, isolated atoms are not a sufficient condition for high activity, as initially atomically dispersed Au^{3+} is inactive and requires an induction period [14].

Improving Au-based catalysts for VCM production will involve the study of methods to highly disperse and subsequently anchor Au in its active form [11] and to this end, Au deposition needs to be studied [5]. Consequently, the goal of the current work is to employ a well-understood deposition method, strong electrostatic adsorption (SEA), to atomically disperse Au precursor complexes on catalyst support surfaces in the course of catalyst synthesis [36]. From this highly dispersed partial monolayer of precursors, we then study the nucleation of Au nanoparticles over various carbon supports with different degrees of surface oxidation as well as oxide supports, as a function of pretreatment and reaction environment. We demonstrate an inverse correlation between nanoparticle anchoring and catalytic activity; oxide supports prevent sintering of Au into large nanoparticles but are inactive. Thus, the role of carbon is critical. However, carbon supports, in varying degrees, do not anchor Au and allow large particles to form very rapidly in the HCl environment, but are more active. The slow deactivation is independent of the initial, rapid particle growth.

2. Experimental

2.1. Materials

Bis(ethylenediamine)gold(III) chloride was used as the cationic gold precursor in all SEA experiments over low PZC supports as it has been shown previously to produce particles with high dispersion supported on carbon and a variety of oxide supports [37]. This gold precursor was synthesized fresh in lab by the method of Block and Bailar [38].

Low PZC supports i.e. oxidized carbon, graphitic carbon, silica, and titania were used as received from the manufacturer in this study to produce one weight percent gold catalysts. The pore volume, PZC and surface area of these supports are summarized in Table 1. Vulcan XC-72 was oxidized using concentrated nitric acid at 85 °C in reflux for 2 h and then rinsed and filtered using DI water until a neutral pH of the filtrate was reached and then calcined in a muffle furnace for 3 h at 400 °C.

2.2.2 pH shifts and PZC measurement

The PZC of the carbon and metal oxide supports were determined using a surface loading of 1000 m^2/L (Eq. (1)) with 50 mL of solution for each sample across all supports, to ensure an equal number of surface sites in solution. Solutions were made at pH values from 1 to 13 using HNO_3 and

Surface loading $(\frac{m^2}{L})$

$$= \frac{\text{Surface Area of support}\left(\frac{m^2}{g}\right)\text{*grams of support(g)}}{\text{Volume of Precursor Solution(L)}} \qquad (1)$$

NaOH to adjust the initial pH. Then 50 mL of each pH-adjusted solution was added to the support in 60-mL polypropylene bottles. The solutions were shaken for 1 h on an orbital shaker at 120 rpm. Final pH measurements were obtained using a general combination pH electrode. At high surface loadings, the plateau of the plotted pH shift corresponds to the PZC [39].

The adsorption of cationic $[Au(en)_2]^{3+}$ onto these low PZC supports was determined as a function of the final pH of the adsorption solutions at constant initial gold concentration. The surface loading was kept constant at 1000 m^2/L and the pH of a solution containing 160 ppm of freshly prepared $Au(en)_2Cl_3$, was adjusted over the pH range of 4–13, using NaOH and HNO_3 to adjust the pH, and the support was then added to obtain the desired surface loading. The 60-ml polypropylene bottles containing 160 ppm $Au(en)_2Cl_3$ solutions and support were shaken for 1 h, after which 5 mL of filtered solution was analyzed for Au content via ICP-OES. The gold uptake was determined as the difference in Au concentrations in the pre- and post-contacted solutions and is reported as surface density, Γ, shown in Eq. (2).

$\Gamma (\mu mol/m^2)$

$$= \frac{(Conc_{inital}(mg/L) - Conc_{final})*10^6 \,(\mu mol/mol)}{\text{Surface Loading } (m^2/L)\text{*}Mw \text{ of Metal } (g/mol)\text{*}1000 \,(mg/g)} \qquad (2)$$

2.3. Catalyst preparation

One gram batches of catalysts of 1.0 wt percent Au were prepared at the pH of maximum uptake (uptake surveys shown later in Fig. 1) where electrostatic forces are strongest. The surface loading was the same as those used for the uptake surveys, and the volume of solution was scaled up to give 1 g catalyst. The Au concentration was limited to the amount needed for a 1.0 wt% catalyst. (In the case of titania, which had low surface area, two cycles of SEA/reduction were employed to achieve 1 wt% Au, as described below in the results.) The weight loading in the scaled up batches was confirmed via ICP-OES analysis of the pre- and post-adsorption solutions. After 1-h contact on the orbital shaker at the optimal pH, the solids were filtered and dried under vacuum overnight. The catalysts were then reduced in flowing 10% H_2 with a balance He at 180 °C and a ramp rate of 3.0 °C/min. Prepared catalysts are stored under vacuum at room temperature until reaction testing and characterization.

A 1.0 wt percent Au/C catalyst was prepared for comparison via conventional incipient wetness impregnation using aqua regia as solvent with untreated VXC-72 carbon as support. A solution of HAuCl4 (Sigma-Aldrich: 50% gold) was dissolved in aqua regia [HCl 37% (Aldrich): HNO3 67% (Aldrich) (3:1)] and this solution was added to the VXC-72 support drop-wise. The prepared catalyst samples were

Table 1
Support materials used in catalytic testing, all supports were used as received, except for the oxidized VXC-72.

Support	Surface Area (m^2/g)	Pore Volume (ml/g)	PZC	Max Au uptake ($\mu mol/m^2$)	Max Au Wt%
HNO_3 Oxidized Vulcan XC-72 carbon (Cabot)	180	1.9	3.7	0.91	3.2
Vulcan XC-72 carbon (Cabot)	254	2.3	8.5	–	
Norit CA-1 carbon (Norit Americas)	1400	1.7	2.6	0.70	19
Darco KB-M carbon (Norit Americas)	1200	3.2	3.5	0.74	17
Darco KB-B carbon (Norit Americas)	1500	4	4.8	0.80	24
Asbury grade 4827 carbon (Asbury Graphite Mills)	115	0.4	4.7	0.70	1.6
Aersoil 300 fumed SiO_2 (Evonik)	330	0.8	3.7	0.55	3.6
Aeroxide P25 TiO_2 (Evonik)	45	0.7	4	0.58	0.5
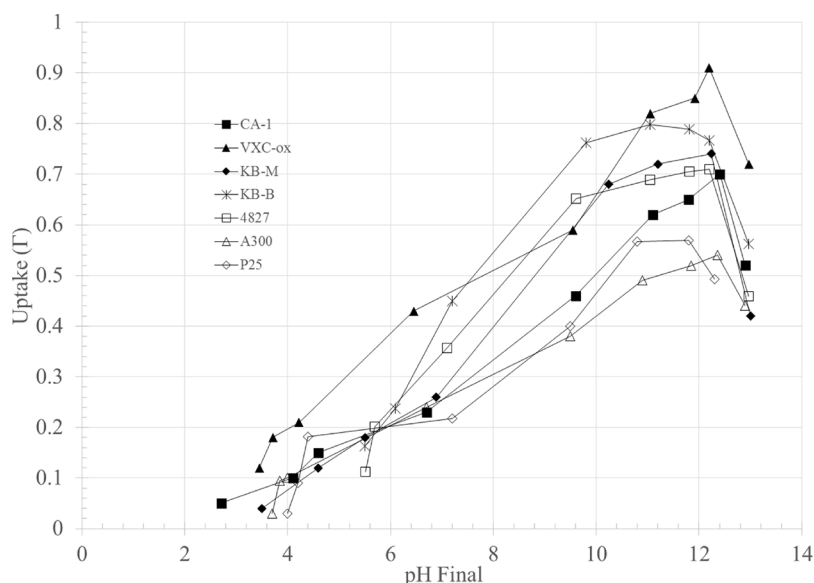
dried overnight and stored under vacuum.

2.4. Catalyst characterization

Powder X-Ray diffraction (XRD) was used to investigate the crystalline characteristics and particle size of the supported gold metal catalysts with a Rigaku Miniflex-II instrument equipped with a D/Tex Ultra detector operating in Bragg–Brentano geometry. The radiation source was Cu-Kα radiation (λ = 1.5406 Å) at 30 kV and 15 mA. All patterns were taken at a scan rate of 0.5°/min and sampling width of 0.02° over the range of $10-80°$ 2θ. The Scherrer equation was used to determine the Au crystalline size with a limit of detection of about 1.5 nm [40]. This analysis was done before and after exposure to HCl and C_2H_2 in the reaction. The analysis of elemental compositions and oxidation states of the catalyst surfaces was determined by x-ray photoelectron spectroscopy (XPS) using a Kratos Axis Ultra DLD instrument equipped with a monochromated Al Kα x-ray source and hemispherical analyzer capable of an energy resolution of 0.5 eV.

2.5. Reaction and particle stability testing

Acetylene hydrochlorination was carried out in a fixed bed glass reactor (i.d. 3/8"). The acetylene gas was treated to remove major inhibiting impurities (acetone) by molecular sieve 5A and mixed with He as well as anhydrous hydrogen chloride gas (Praxair; 99.999%), before being fed to the reactor using calibrated mass flow controllers for each gas. Prior to the start of the reaction, the reduced catalysts were dried at 110 °C for 1 h under flowing He and then pre-chlorinated with mixed helium and hydrogen chloride gas at 1:1 flow ratios at 180 °C for 1 h. As previous work has shown, the initial surface composition ratio of $AuCl_x:Au^0$ can be maximized by this prechlorination [8,10,41]. Acetylene was then fed through the reactor containing the pre-chlorinated catalysts at helium to acetylene to hydrochloride ratios of 1:1:1.1 at 180 °C with a HCl flow of 11 SCCM standard cubic centimeters per minute (SCCM) for a GHSV of 4500 h^{-1}. The exit gas from the reactor was passed through a concentrated NaOH solution to eliminate non-reacted hydrogen chloride and the scrubbed gaseous products were analyzed by an on-line GC (HP5890 FID detector using an Agilent J&W HP-Plot Q capillary Poraplot Q column). The fractional conversion of C_2H_2 was determined using the standard formalism of $(C_{2}H_{2(in)}-C_{2}H_{2(out)})/C_{2}H_{2(in)}$. VCM selectivity was calculated from the amount of VCM formed/amount of total products formed. All catalysts showed high selectivity to vinyl chloride (> 99.5%) at a GHSV of

4500 h^{-1} with only trace amounts of the C_2 side product 1–2 dichloroethane being observed. For testing of gold particle stability, the samples were dried under the same conditions as reaction samples and then HCl in He was added to the reactor cell for the desired time. For low HCl concentration experiments, 100 ppm and 2000 ppm HCl diluted in a balance of He was used.

3. Results and discussion

3.1. Au deposition, nanoparticle synthesis and characterization

The PZC of carbons used in the present study ranged from 2.6 to 4.8; measured values of the support properties are given in Table 1. The PZC's were measured by equilibrium pH at high oxide loading (EpHL) experiments; details can be found elsewhere [39]. Gold uptake (Γ vs pH$_{final}$) over the various supports versus pH is shown in Fig. 1 and exhibits the typical SEA volcano shape, indicating that metal adsorption mechanism is electrostatic. As the solution becomes highly basic, the increase in ionic strength of the solution retards metal adsorption. For all complexes an optimal final pH near 12 is observed with maximum uptake values that range from 0.55–0.9 μmol/m^2. The metal uptake at values close to the acidic PZCs of the supports gave limited uptake as there was insignificant surface charge and thus no driving force for electrostatic adsorption. Gold uptake for the activated and graphitic carbons (CA-1, KB-M, KB-B, and VXC-ox, 4827) is slightly higher compared to the oxide supports (A300 and P25), though they all have similarly acidic PZC's; this variance may have been a result of inaccuracies in the BET surface area measurements. The maximum uptake over each support and the corresponding maximum Au weight% achievable in a single SEA deposition are summarized in Table 1.

Shifts in pH from a metal free control experiment were very similar to the metal-containing experiments for the different carbons and oxide supports (data not shown). The similarity of the two sets of data confirms an electrostatic adsorption mechanism, in which surface charging is assumed to be independent of metal adsorption [42].

As detailed in the experimental section, one gram batches of gold catalyst were synthesized using each support at the pH of optimum uptake to produce one weight percent Au samples. Powder x-ray diffraction experiments were conducted on the fresh, reduced samples before reaction (and prior to HCl contact), as well as on the spent catalyst after 20 h of time on stream (TOS). These results are shown in Fig. 2 and are summarized in Table 2.

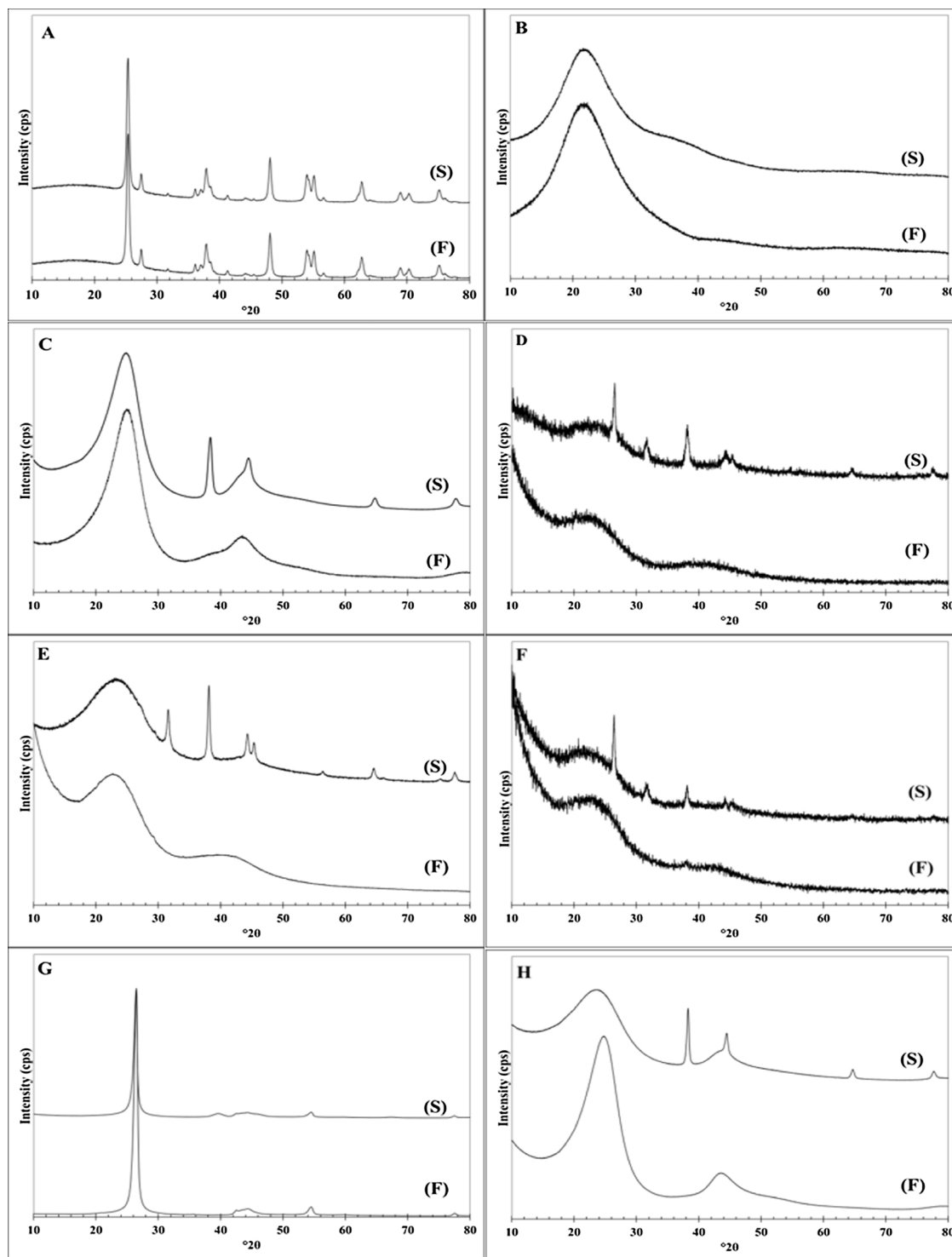The particle size of most of the fresh samples (the bottom pattern of

Fig. 2. XRD patterns for the fresh (F) and spent (S) catalyst samples. A) P25, B) A300, C) VXC−OX, D) KB-M, E) KB-B, F) CA-1, G) 4827H) VXC-IWI. Au (111) position: 38.3°2θ.

each part of Fig. 2) were below the limit of XRD detection; for the CA-1, KB-M and KB-B samples, broad peaks were observed with sizes estimated to be 2.0, 3.0, and 2.1 nm respectively. The dramatic growth in the particle sizes of the spent carbon-supported catalysts is seen by the emergence of sharp XRD peaks in the post-reaction catalysts (upper patterns). Particle sizes over carbon were generally in the range of 20 nm. A final observation from Fig. 2 is that crystalline NaCl appeared in all used activated carbons, most likely forming from the Na impurity typical of this type of carbon. The dependence of sintering on support will be discussed after the reactivity results are presented.

The STEM images of the fresh and aged Au/KBB catalyst in Fig. 3 show the small size of the fresh Au nanoparticles (Fig. 3a) including the presence of many individual Au atoms in a highly magnified image (Fig. 3b). The spent sample consists mainly of sintered particles (Fig. 3c) but in some areas, individual atoms still appear (Fig. 3d).

3.2. Reactivity of carbon and oxide supported catalysts

Reactivity results are shown in Fig. 4. Of immediate note is the relative inactivity of Au supported on the two oxides, P25 and A300,

Table 2
Particle size before and after 20 hours TOS for Au catalysts at a GHSV of 4500 hr^{-1} with a 1.1:1:1 ratio of HCl:C_2H_2:He

Catalyst	Notation	Fresh Particle Size (nm)	Spent Particle Size (nm)
1 wt.% Au/VXC-ox	VXC-ox	< 1.5	12
1 wt.% Au/VXC (IWI)	VXC	< 1.5	16
1 wt.% Au/CA-1	CA-1	2	20
1 wt.% Au/KB-M	KB-M	3	18
1 wt.% Au/KB-B	KB-B	2.1	22
1 wt.% Au/4827	4827	< 1.5	3.7
1 wt.% Au/A300	A300	< 1.5	< 1.5
1 wt.% Au/P25-TiO$_2$	P25	< 1.5	< 1.5

and the unoxidized carbon, 4827. All non-graphitic carbon-supported gold catalysts had similar conversion patterns; initial high conversion likely stemming from completely oxidized Au^{3+} resulting from the HCl-rich pretreatment, followed by a rapid deactivation over the first 0–5 h and then a slower decay over the remainder of time on-line. The VXC-ox and the VXC-iwi samples showed the highest initial activities with conversions of about 50 percent. However, the VXC-ox sample had the slowest decay rate of conversion while the VXC-iwi sample exhibited the highest long term decay rate. The rest of the carbon supports, i.e. CA-1, KB-M, and KB-B show similar trends to the VXC-ox carbon albeit with slightly lower conversion values, but similar, slow, long term deactivation trends

The long term activities of approximately 30% conversion at a GHSV of 4500 h^{-1} is about the same as those observed in earlier work using the same flow system, in which long term conversions of about 80% were noted for the same Au weight loading (1 wt%) at about a third of the space velocity (1480 h^{-1}) [10]. These activities are considerably higher than for similar 1 wt% Au/C catalysts that gave conversion of 70% at a lower space velocity of 740 h^{-1} [3,8]. The higher space velocity in the current work was chosen to more closely mimic industrial conditions and to better observe deactivation trends during time on line. Another benchmark in activity can be made with the aged catalysts of the low loading catalysts in Fig. 10 of [11]. Based on their flow conditions and the amount of catalyst they employed, space time yields of VCM after 175 h of aging ranged from 1.3 to 1.6 kg VCM/(kg catalyst h), with the 1 wt% Au catalyst having a STY of 1.5 kg VCM/(kg catalyst h) [11]. The highest activity observed in Fig. 4, for the 1 wt% Au on oxidized VXC support (after only 20 h of aging) was 2.8 kg VCM/(kg catalyst h). Converted to per kg Au, the STYs in [11] ranged from 150 to 850 kg VCM/(kg Au h), with the 1 wt% Au catalyst having the lowest STY and the lowest gold loading, the 0.15%, having the highest.
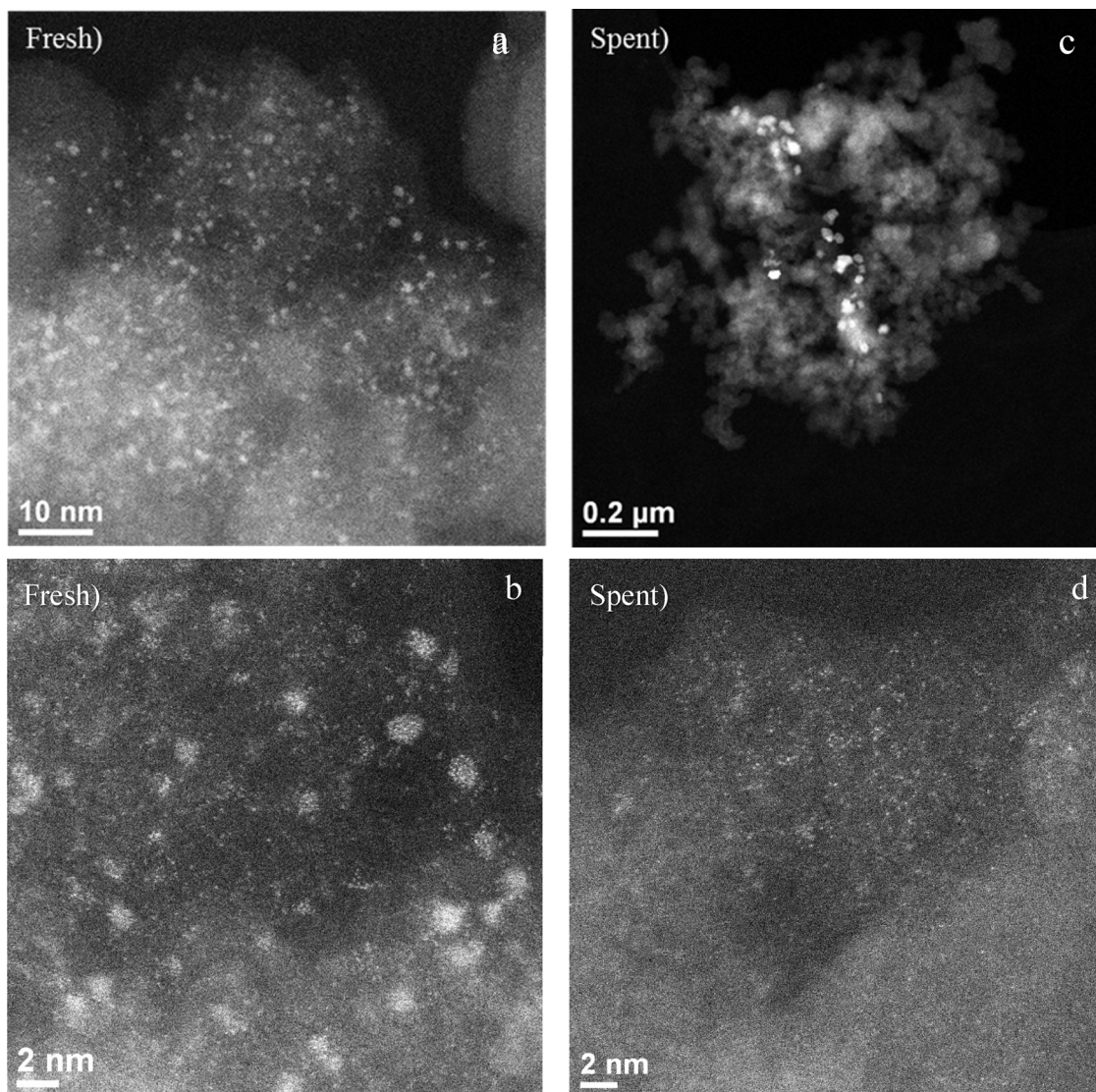

Fig. 3. Representative STEM images of the Au/KBB catalyst, fresh (a and b) and after 20 h on stream (c and d).
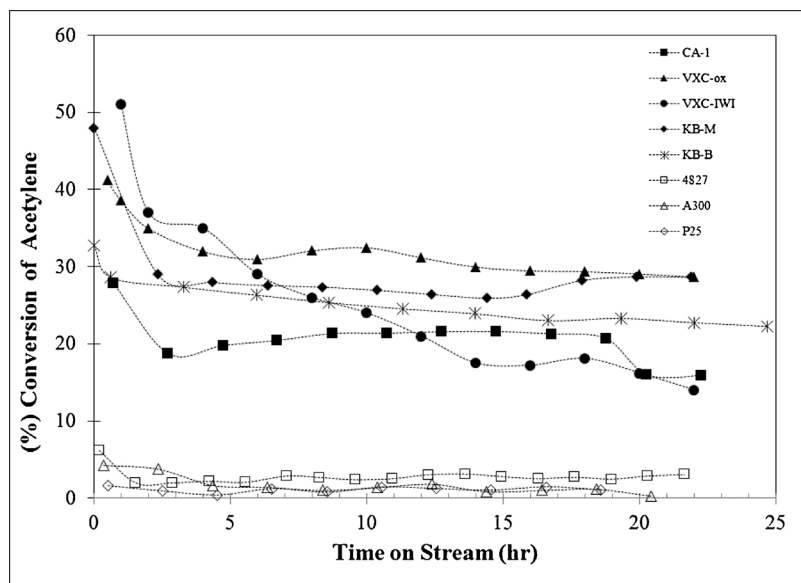
(We note in [11] that Au appears to be the best utilized in the lowest loading catalyst.) The Au-based STY of the 1 wt% Au/VXCox catalyst in Fig. 4 is 280 kg VCM/(kg Au h).

Characterization of the used catalysts is given in Figs. 2 and 3 and is summarized in Table 2. The XRD results reveal that the different supports exhibited vastly different anchoring of the Au particles. Sharp Au peaks indicated that extensive sintering occurred over all carbon supports except the graphitic carbon, which sintered only mildly, whereas the absence of Au peaks over the oxide supports indicates the strong anchoring of gold particles to these surfaces. The STEM image of the aged Au/KBB catalyst in Fig. 3c confirms the sintering of Au particles.

An intriguing trend is seen in comparing the post reaction characterization data to the activity data in Fig. 4; the spent catalysts that gave the highest activities were generally those samples which sintered the most. The silica, titania, and graphitic carbon samples which showed no or minimal Au sintering were the least active catalysts for acetylene hydrochlorination. This trend holds even within this subgroup; of the three least active catalysts the highest activity, the graphitic carbon-supported Au catalyst was most active and did show some sintering (see Au peak evolution in Fig. 2) while the A300 silica-supported Au sample with intermediate activity, showed a trace of sintering, and the least active P-25 TiO$_2$-supported Au catalyst showed virtually no sintering.

Of the group of most active catalysts (the activated carbons and carbon blacks), it is noteworthy that activity does not track well with particle size. The KB-M and VXC-ox samples have similar conversions of 30% after 20 h of run time even though particle sizes differ by 50% (12 and 18 nm, respectively, in Table 2). The activated carbons and the oxidized carbon black all exhibit relatively slow rates of deactivation, while the unoxidized VXC catalyst displays a continual deactivation through 20 h. This differs notably from the oxidized VXC-ox sample. A number of studies have related stability to the degree of oxidation of the support [5,27,29,32,35] and these data are consistent with them.

A final set of pre- and post-reaction characterizations was performed using XPS (Fig. 5) for fresh and spent samples of Au supported on (VXC-ox) using both SEA and HAuCl$_4$ impregnation (VXC-iwi) methods, after reduction but before reaction. The normal 4f binding energies of Au^0 are approximately 84 and 87 eV for Au4f$_{7/2}$ and Au5$_{f/2}$, respectively, while the Au4f$_{7/2}$ and Au5$_{f/2}$ peaks for Au^{3+}, widely assumed to be the active species in this reaction [5,10], have values of 86 and 89 eV, respectively [43]. Not unexpectedly, no Au^{3+} was detected on the surfaces of the freshly reduced catalyst samples prepared via SEA or IWI; neither was Au^{3+} observed for the spent catalysts, consistent with XRD
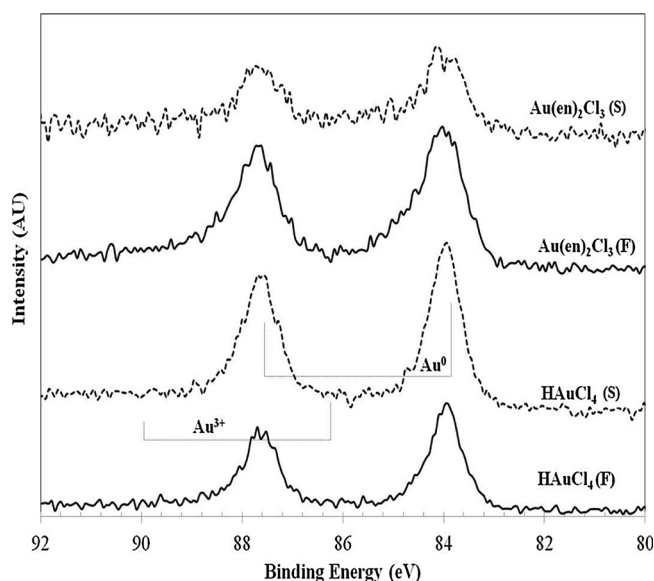

Fig. 5. XPS spectra of fresh (F) and spent (S) Au/C catalysts using HAuCl$_4$ prepared via IWI and Au(en)$_2$Cl$_3$ prepared via SEA. Binding energy values have been referenced to C1 s peak at 284.6 eV.

analyses for spent Au catalysts having large particle sizes [35,44,45]. These results imply that the number of active Au^{3+} sites must be small compared to the total number of Au sites and that deactivated catalysts consist basically of large particles of sintered Au^0.

3.3. Au sintering studies

The effects on gold sintering of temperature and HCl exposure were isolated in a separate series of experiments. In many cases HCl is used to reactivate used catalysts [3], many of which feature large, sintered particles. Here, we start with the ultrasmall Au particles produced from SEA to determine the effect of the prechlorination step on them. XRD results in Fig. 6 show the effects of temperature only, and with HCl exposure at temperature on 1 wt% Au/KBB carbon for different lengths of time. A fresh sample of 1 wt% Au/KBB catalyst was reduced at standard conditions in flowing 10% H$_2$ with a balance He at 180 °C and a ramp rate of 3.0 °C/min. The reduced samples were pretreated in flowing He (10 SCCM) for 20 h at 180 °C before XRD analysis. This
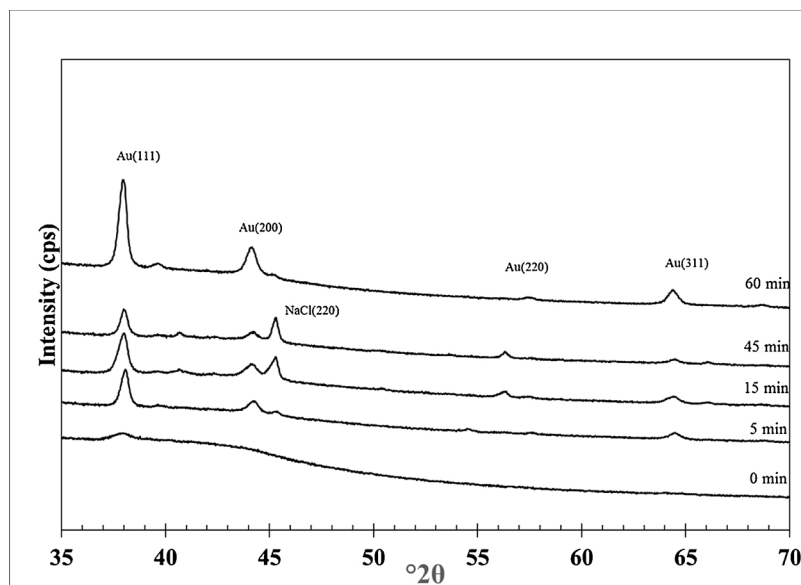
sample, shown as the bottom XRD pattern in Fig. 6, did not exhibit Au peaks, indicating high stability of the Au^0 nanoparticles in He at 180 °C. Additional samples were pre-reduced as before and then contacted with 50% HCl/balance He for 5, 15, 45 and 60 min. Substantial sintering was observed even after 5 min exposure to HCl; size estimates from the Au (111) peak widths were 21, 19, 20, and 21 nm for the respective times. This is essentially the same size as the post-reaction KB-B sample (Table 2). Thus it appears that HCl exposure and not temperature causes the Au particles to undergo rapid sintering during the hydrochlorination of C_2H_2. Notably, only the peak intensities grew with continued times of exposures; peak widths remained more or less constant. For example, after 5 min exposure to the 50% HCl/balance He gas stream the Au peak intensity was about one half of that for one hour of exposure, implying that half of the Au remains as small particles, perhaps even atomically dispersed, below the limit of detection of the diffractometer while the other half exists as 20 nm particles. In similar fashion, a VXC-ox sample monitored at 30, 60, 120 and 240 min after reaction (not shown) exhibited constant peak breadth corresponding to a particle size of 11 nm (consistent with Table 2) while the intensity grew in time. This manner of particle growth a mechanism of rapid sintering to a stable size once a particle has been nucleated, i.e., growth occurs faster than nucleation. This same sort of Au particle growth, showing similar-width Au fcc peaks, but of growing intensity, was observed by Dai et al. [35]. That group, however, did not report the pretreatment time, making it difficult to correlate activity with particle size in that report. The data in the present study shows that sintering rapidly occurs during pretreatment, within the first few minutes in the 50% HCl flow. After the one hour prechlorination, prior to the reaction data shown in Fig. 4, all catalysts will have reached their large and stable particle size, after which Au particle sizes remain essentially constant as deactivation slowly occurs over the 24 h of catalyst evaluation.

To further determine the sensitivity of sintering to gas phase HCl, 1 wt% Au/VXC-ox pre-reduced samples were exposed to 10 SCCM dilute HCl (100 ppm or 2000 ppm) in a balance of He at 180 °C after a one hour purge in He at the same temperature. Running the 100 ppm HCL steam for 10 and 30 min gave a total exposure of Au in ratios of 3:1 HCl:Au and 9:1 HCl:Au, while running the 2000 ppm stream for 25, 80, and 300 min gave exposures of 170:1, 630:1, and 2500:1 HCl:Au. After the HCl exposures, the flow of HCl was stopped and the system purged with He, cooled to 25 °C, and the sample removed for XRD analysis. The results are shown in Fig. 7.

XRD patterns of samples exposed to 3:1 and 9:1 HCl:Au ratios,

showed no change from the He-annealed sample which was stable to the 180 °C He flow for 20 h. However, as the HCl:Au ratio increased from 170:1 for 25 min to 2500:1 for 300 min, there is a noticeable increase in Au particle size induced by the HCl exposure. Particle sizes for exposures of HCl:Au ratios of 630:1 and 2500:1 were 4.1 nm and 7.6 nm, respectively, which were still considerably smaller than the Au^0 particle sizes of 12 nm observed for the same catalyst after 20 h of reaction in a gas flow of 33% HCl with balance of C_2H_2 and He. For perspective, after 20 h under reaction conditions, the ratio of HCl to Au is on the order of 620,000.

3.4. Implications on active sites

The least active catalysts were those with the smallest Au nanoparticles and therefore the highest number of metal surface atoms; catalytic activity cannot be correlated to metallic Au area within the set of carbons, or considering all carbon and oxide supports. Nor can the activity be correlated to the perimeter length of metal crystallites (the number of sites at the particle-support interface). In light of the recent, thorough operando XAS evidence of Hutchings et al. for isolated Au being the active site [15], we would surmise that 1) the metal particles observable by XRD are wholly inactive, 2) activity is imparted by hard-to-observe atomically dispersed Au ions, and 3) the slow deactivation on carbon comes from atomically dispersed Au migrating and attaching to large metal particles. The presence of difficult-to-observe but highly active isolated Au sites may explain the activity attributed (mistakenly) to metallic Au in VCM catalysts containing mainly metallic nanoparticles [35]. The high magnification STEM images of the fresh and spent 1 wt% Au/KBB sample used here (Figs. 3b and d respectively), reveal a significant fraction of isolated Au atoms in the fresh state (Fig. 3b) and also some isolated Au in the spent state (Fig. 3d), to which the catalytic activity can be attributed. While the fraction of isolated gold could not be quantified from these images, continued work is underway with controlled series of catalysts precisely to correlate the degree of atomically dispersed Au with the degree of controlled carbon oxidation, and relating both of these to catalyst deactivation.

Hutching's method of incipient wetness of low loadings of $HAuCl_4$ in aqua regia [11,15], yields isolated, chlorided Au ions at the outset of synthesis. On the other hand, the cationic ethylenediamine Au complex used here for SEA with low PZC supports must have the ligands replaced with chloride before use. The initial reduction used to accomplish this generated nanoparticles, though small (usually below the limit of our XRD detection), but nanoparticles nonetheless. These will
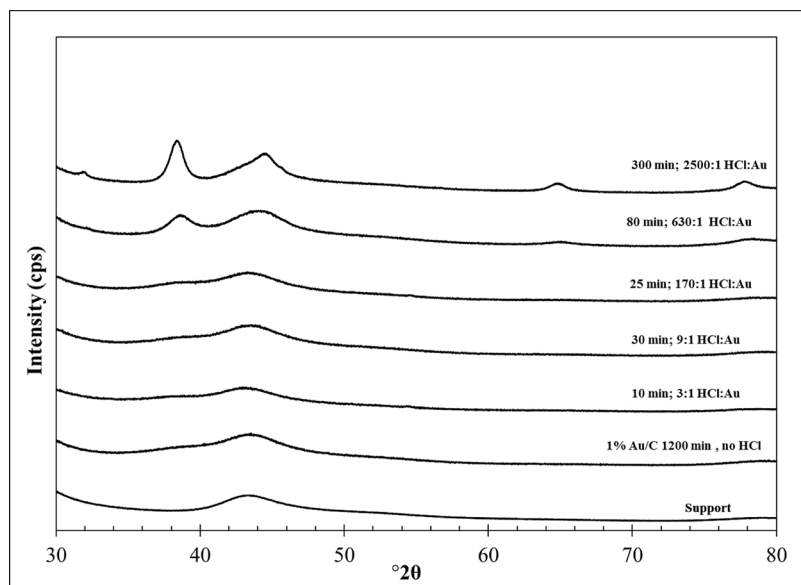
Fig. 7. XRD patterns of samples after exposure to 10 SCCM total flow rate of HCl/balance He at 180 °C for the times shown in the legend. The 10 and 30 min exposures were made using 100 ppm HCl/balance He, and the 25, 80, and 300 min exposures used 2000 ppm HCl/balance He. Au (111) position: 38.3°2θ.

act as nucleation sites during the chlorination step, lessening the amount of isolated Au. Therefore, synthesis via deposition of non-chloride Au species appears disadvantageous compared to a method in which it deposited in a well dispersed manner in the chloride form or as a different ligated ion that will undergo facile ligand exchange with Cl⁻ during reaction. We do note that the most active catalyst support, with the smallest sintered particle size, is oxidized VXC (VXC-ox), which is known to contain about $0.3 - 0.5$ atomic% sulfur [46,47]. However, over VXC without the surface oxygen, the Au deactivates much more severely. On the whole, the high fraction of metal generated by reduction after SEA renders any remaining isolated Au practically unobservable.

Neither of the oxides employed resulted in an active Au catalyst. This has been reported previously for Au on a pure titania support [16] but rarely otherwise. The inactivity of well dispersed Au on oxide supports implies that either an insignificant fraction of the Au ions are isolated over the oxides, which is not likely given that via SEA the Au begins as an atomically dispersed precursor over all supports, or, that carbon is necessary for the active site. Curiously, not any carbon will suffice; the graphitic carbon employed here (4827) resulted in an inactive catalyst with good anchoring ability, while the carbon black (VXC) and activated carbons (CA-1, KB-M and KB-B) were active but sintered. The importance of the carbon surface oxygen groups in stabilizing activity for acetylene hydrochlorination has been reported numerous times [5,28,33], but these did not test graphitic carbon. The particle size of the spent graphitic sample, at 3.7 nm, has a perimeter length of about an order of magnitude greater than the other spent carbon catalysts of about 20 nm in size. This argues that it is not simply Au adjacent to any carbon at the edges of metallic nanoparticles [32] that becomes oxidized and active, but rather Au adjacent to (or isolated on) amorphous carbon. In light of the recent demonstration of isolated sites [15] and a lack of correlation of activity with perimeter sites of the amorphous carbons used in this study (Fig. 4), it is more likely that the active sites are isolated and not perimeter sites. Graphitic carbon is highly ordered, as seen in the graphite XRD peaks of Fig. 4G. That Au sinters less over a well-structured surface with smooth basal planes, as opposed to the oxidized and defect-laden amorphous surfaces of the blacks and activated carbons is counterintuitive. This suggests, firstly, that the oxygen groups of the oxidized blacks and activated carbons are different from characteristic oxygen groups on graphitic carbon and are necessary for high activity. The chemical specificity of O functional groups on carbon may also explain why aqua regia activates and stabilizes catalysts better than HCl or nitric acid alone [5]. Secondly, since

it is the active catalysts which sinter, the active species must be mobile. One path to deactivation may be the formation of the dimer of $AuCl_3$, or Au_2Cl_6, which Rustad and Gregory [48] observed as a product from the reaction of Au^0 with HCl at temperatures similar to those used for hydrochlorination of C_2H_2. They used UV–vis spectroscopy and the unique absorption bands for gas phase Au_2Cl_6 at 222 and 244 nm to detect the formation of volatile Au_2Cl_6 from Au^0 and gas phase HCl. No other volatile $AuCl_x$ species were observed, and the only other products formed in smaller amounts were non-volatile AuCl and gas phase Cl_2. Some dimers were observed in Hutching's low loading catalysts (Fig. S15 of [15]); it is perhaps the role of the S-containing ligands to prevent their formation.

4. Conclusions

Cationic gold ethylenediamine complexes have been deposited in a controlled manner, as partial monolayers, over a variety of carbon and oxide surfaces. To convert the precursors to active catalysts for acetylene hydrochlorination, the precurors were reduced in hydrogen and then chlorinated in HCl/He. The reduction resulted in the genesis of highly dispersed Au nanoparticles (usually below the 1.5 nm limit of detection and some from 2 to 3 nm) over all supports. The series of catalysts exhibited an unusual relationship of sintering to activity; the catalysts which best anchored the Au crystallites were the least active; titania and silica catalysts showed almost no sintering and were virtually inactive, and even a graphitic carbon catalyst exhibited good anchoring but very poor activity. The sintering was caused by the HCl atmosphere and not the temperature; catalysts submitted to the reaction temperature in He were stable.

It would appear that the metal nanoparticles, and perhaps also the Au at the edges of metal nanoparticles at the metal/carbon interface, are inactive. High resolution images of fresh and spent catalyst both contain atomically dispersed Au and support recent literature that the active sites are derived from isolated Au ions. We can further conclude that oxidized amorphous carbon plays a key role in generating the active site. Yet in this environment, the active species is highly mobile and susceptible to sintering.

Acknowledgements

References

[1] J.G. Speight, Chemical and Process Design Handbook 2 McGraw-Hill, 2002, pp. 20–22 (22).

[2] M. Conte, A.F. Carley, G. Attard, A.A. Herzing, C.J. Kiely, G.J. Hutchings, Hydrochlorination of acetylene using supported bimetallic Au-based catalysts, J. Catal. 257 (2008) 190–198.

[3] B. Nkosi, N.J. Coville, G.J. Hutchings, M.D. Adams, J. Friedl, F.E. Wagner, Hydrochlorination of acetylene using gold catalysts: a study of catalyst deactivation, J. Catal. 128 (1991) 366–377.

[4] N.L. Jinli Z.H.A.N.G, L.I. Wei, D.A.I. Bin, Progress on cleaner production of vinyl chloride monomers over non-mercury catalysts, Front. Chem. Sci. Eng. 5 (2011) 514–520.

[5] M. Conte, C.J. Davies, D.J. Morgan, T.E. Davies, D.J. Elias, A.F. Carley, P. Johnston, G.J. Hutchings, Aqua regia activated Au/C catalysts for the hydrochlorination of acetylene, J. Catal. 297 (2013) 128–136.

[6] G.J. Hutchings, Catalysis by gold, Catal. Today 100 (2005) 55–61.

[7] G.J. Hutchings, Gold catalysis in chemical processing, Catal. Today 72 (2002) 11–17.

[8] B. Nkosi, M.D. Adams, N.J. Coville, G.J. Hutchings, Hydrochlorination of acetylene using carbon-supported gold catalysts: a study of catalyst reactivation, J. Catal. 128 (1991) 378–386.

[9] X. Tian, G. Hong, B. Jiang, F. Lu, Z. Liao, J. Wang, Y. Yang, Efficient Au 0/C catalyst synthesized by a new method for acetylene hydrochlorination, RSC Adv. 5 (2015) 46366–46371.

[10] W. Wittanadecha, N. Laosiripojana, A. Ketcong, N. Ningnuek, P. Praserthdam, J.R. Monnier, S. Assabumrungrat, Preparation of Au/C catalysts using microwave-assisted and ultrasonic-assisted methods for acetylene hydrochlorination, Appl. Catal. A: Gen. 475 (2014) 292–296.

[11] P. Johnston, N. Carthey, G.J. Hutchings, Discovery development, and commercialization of gold catalysts for acetylene hydrochlorination, J. Am. Chem. Soc. 137 (2015) 14548–14557.

[12] K. Zhou, J.C. Jia, C.H. Li, H. Xu, J. Zhou, G.H. Luo, F. Wei, A low content Au-based catalyst for hydrodechlorination of C2H2 and its industrial scale-up for future PVC processes, Green Chem. 17 (2015) 356–364.

[13] M.Y. Zhu, Q.Q. Wang, K. Chen, Y. Wang, C.F. Huang, H. Dai, F. Yu, L.H. Kang, B. Dai, Development of a heterogeneous non-mercury catalyst for acetylene hydrochlorination, ACS Catal. 5 (2015) 5306–5316.

[14] X. Liu, M. Conte, D. Elias, L. Lu, D.J. Morgan, S.J. Freakley, P. Johnston, C.J. Kiely, G.J. Hutchings, Investigation of the active species in the carbon-supported gold catalyst for acetylene hydrochlorination, Catal. Sci. Tech 6 (2016) 5144–5153.

[15] G. Malta, S.A. Kondrat, S.J. Freakley, C.J. Davies, L. Lu, S. Dawson, A. Thetford, E.K. Gibson, D.J. Morgan, W. Jones, P.P. Wells, P. Johnston, C.R.A. Catlow, C.J. Kiely, G.J. Hutchings, Identification of single-site gold catalysis in acetylene hydrochlorination, Science 355 (2017) 1399–1403.

[16] C. Huang, M. Zhu, L. Kang, X. Li, B. Dai, Active carbon supported TiO2-AuCl3/AC catalyst with excellent stability for acetylene hydrochlorination reaction, Chem. Eng. J. 242 (2014) 69–75.

[17] S. Mitchenko, T. Krasnyakova, I. Zhikharev, Catalytic hydrochlorination of acetylene on mechanochemically-activated K2PdCl4, Theor. Exp. Chem. 44 (2008) 316–319.

[18] S. Wang, B. Shen, Q. Song, Kinetics of acetylene hydrochlorination over bimetallic Au-Cu/C catalyst, Catal. Lett. 134 (2010) 102–109.

[19] S.A. Mitchenko, T.V. Krasnyakova, R.S. Mitchenko, A.N. Korduban, Acetylene catalytic hydrochlorination over powder catalyst prepared by pre-milling of K2PtCl4 salt, J. Mol. Catal. A- Chem. 275 (2007) 101–108.

[20] R.S. Mitchenko, A.A. Shubin, T.V. Krasnyakova, Mechanism of the catalytic action of the mechanoactivated salt K 2PTCL4 in the gas-phase hydrochlorination of acetylene, Theor. Exp. Chem. 42 (2006) 314–319.

[21] J. Ma, S. Wang, B. Shen, Study on the effects of acetylene on an Au–Cu/C catalyst for acetylene hydrochlorination using monte carlo and DFT methods, Reac Kinet Mech Cat 110 (2013) 177–186.

[22] G. Li, W. Li, H. Zhang, Y. Pu, M. Sun, J. Zhang, Non-mercury catalytic acetylene hydrochlorination over Ru catalysts enhanced by carbon nanotubes, RSC Adv. 5 (2015) 9002–9008.

[23] Y. Pu, J. Zhang, L. Yu, Y. Jin, W. Li, Active ruthenium species in acetylene hydrochlorination, Appl. Catal. A: Gen. 488 (2014) 28–36.

[24] J. Zhang, W. Sheng, C. Guo, W. Li, Acetylene hydrochlorination over bimetallic Ru-based catalysts, RSC Adv. 3 (2013) 21062–21068.

[25] K. Zhou, J. Jia, X. Li, X. Pang, C. Li, J. Zhou, G. Luo, F. Wei, Continuous vinyl chloride monomer production by acetylene hydrochlorination on Hg-free bismuth catalyst: from lab-scale catalyst characterization catalytic evaluation to a pilot-scale trial by circulating regeneration in coupled fluidized beds, Fuel Process. Technol. 108 (2013) 12–18.

[26] B. Dai, K. Chen, Y. Wang, L. Kang, M. Zhu, Boron and nitrogen doping in graphene for the catalysis of acetylene hydrochlorination, ACS Catal. 5 (2015) 2541–2547.

[27] X. Li, Y. Wang, L. Kang, M. Zhu, B. Dai, A novel, non-metallic graphitic carbon nitride catalyst for acetylene hydrochlorination, J. Catal. 311 (2014) 288–294.

[28] J. Gu, Q. Du, Y. Han, Z. He, W. Li, J. Zhang, Nitrogen-doped carbon supports with terminated hydrogen and their effects on active gold species: a density functional study, Phys. Chem. Chem. Phys. 16 (2014) 25498–25507.

[29] X. Li, M. Zhu, B. Dai, AuCl3 on polypyrrole-modified carbon nanotubes as acetylene hydrochlorination catalysts, Appl. Catal. B: Environ. 142–143 (2013) 234–240.

[30] M. Conte, A.F. Carley, C. Heirene, D.J. Willock, P. Johnston, A.A. Herzing, C.J. Kiely, G.J. Hutchings, Hydrochlorination of acetylene using a supported gold catalyst: a study of the reaction mechanism, J. Catal. 250 (2007) 231–239.

[31] J. Xu, J. Zhao, J. Xu, T. Zhang, X. Li, X. Di, J. Ni, J. Wang, J. Cen, Influence of surface chemistry of activated carbon on the activity of gold/activated carbon catalyst in acetylene hydrochlorination, Ind. Eng. Chem. Res. 53 (2014) 14272–14281.

[32] M. Conte, C.J. Davies, D.J. Morgan, T.E. Davies, A.F. Carley, P. Johnston, G.J. Hutchings, Modifications of the metal and support during the deactivation and regeneration of Au/C catalysts for the hydrochlorination of acetylene, Catal. Sci. Technol. 3 (2013) 128–134.

[33] J. Zhao, J. Xu, J. Xu, T. Zhang, X. Di, J. Ni, X. Li, Enhancement of Au/AC acetylene hydrochlorination catalyst activity and stability via nitrogen-modified activated carbon support, Chem. Eng. J. 262 (2015) 1152–1160.

[34] K. Zhou, W. Wang, Z. Zhao, G. Luo, J.T. Miller, M.S. Wong, F. Wei, Synergistic gold–bismuth catalysis for non-mercury hydrochlorination of acetylene to vinyl chloride monomer, ACS Catal. 4 (2014) 3112–3116.

[35] B. Dai, Q. Wang, F. Yu, M. Zhu, Effect of Au nano-particle aggregation on the deactivation of the AuCl3/AC catalyst for acetylene hydrochlorination, Sci. Rep. 5 (2015).

[36] S.E.A. chapter.

[37] S.E. Barnes, Ph.D. Thesis, Optimization of Single and Bimetallic Noble Metal Catalysts by Strong Electrostatic Adsorption, U. Illinois at Chicago., 2011.

[38] B.P. Block, J.C. Bailar, The reaction of gold(III) with some bidentate coördinating groups1, J. Am. Chem. Soc. 73 (1951) 4722–4725.

[39] J. Park, J.R. Regalbuto, A simple, accurate determination of oxide PZC and the strong buffering effect of oxide surfaces at incipient wetness, J. Colloid Interface Sci. 175 (1995) 239–252.

[40] K. O'Connell, J.R. Regalbuto, High sensitivity silicon slit detectors for 1 nm powder XRD size detection limit, Catal. Lett. 145 (2016) 777–783.

[41] G.J. Hutchings, Vapor phase hydrochlorination of acetylene: correlation of catalytic activity of supported metal chloride catalysts, J. Catal. 96 (1985) 292–295.

[42] X. Hao, W. Spieker, J. Regalbuto, A further simplification of the revised physical adsorption (RPA) model, J. Colloid Interface Sci. 267 (2003) 259–264.

[43] Z. Chen, Q. Gao, Enhanced carbon monoxide oxidation activity over gold–ceria nanocomposites, Appl. Catal. B: Environ. 84 (2008) 790–796.

[44] X. Tian, G. Hong, B. Jiang, F. Lu, Z. Liao, J. Wang, Y. Yang, Efficient Au0/C catalyst synthesized by a new method for acetylene hydrochlorination, RSC Adv. 5 (2015) 46366–46371.

[45] W. Wittanadecha, N. Laosiripojana, A. Ketcong, N. Ningnuek, P. Praserthdam, J. Monnier, S. Assabumrungrat, Preparation of Au/C catalysts using microwave-assisted and ultrasonic-assisted methods for acetylene hydrochlorination, Appl. Catal. A: Gen. 475 (2014) 292–296.

[46] W.S. Baker, J.W. Long, R.M. Stroud, D.R. Rolison, Sulfur-functionalized carbon aerogels: a new approach for loading high surface area electrode nanoarchitectures with precious metal catalysts, J. Non-Cryst. Sol. 350 (2004) 80–87.

[47] D. Pantea, H. Darmstadt, S. Kaliaguine, L. Summchen, C. Roy, Electrical conductivity of thermal carbon blacks: influence of surface chemistry, Carbon 39 (2001) 1147–1158.

[48] D.S. Rustad, N.W. Gregory, The ultraviolet-visible absorption spectrum of dimeric gold(III) chloride in the gas phase. An equilibrium study of vapours formed by gold-chlorine-water mixtures, Polyhedron 10 (1991) 633–643.